Conference Proceedings

Solar World Congress 2015
Daegu, Korea, 08 – 12 November 2015

Experimental Set-up for Investigation of Air-Flow and Dust Deposition in Heliostat Field: Design and Evaluation

Nibodh Boddupalli, Navneet Kumar Yadav and Laltu Chandra[1]

Indian Institute of Technology Jodhpur, Jodhpur (India)

[1]Correspondence author: chandra@iitj.ac.in

Abstract

In this paper, design and evaluation of an experimental setup for analyzing air-flow and to understand dust deposition on heliostats in a field-layout is presented. For this purpose, a heliostat field is designed and air-flow is investigated for the selected staggered arrangement of heliostats. The evaluation clearly revealed the presence of flow separation and wake behind an inclined heliostat models. Such complex flow field will affect dust deposition on heliostat and may even induce vibration. Hence, experimentation would be necessary to investigate the flow field in these regions. The developed experimental set-up based on detailed flow analysis will be useful for understanding the dust deposition and wake induced vibration of heliostats in field layout.

Keywords: *Experimental Set-up Design, Dust Deposition, Heliostat Field, LDV, CFD, RANS & LES*

1. Introduction

Depleting conventional sources of non-renewable energy has been one of the key reasons for research into alternate sources of energy like solar energy. There are different methods to harness solar energy. One of them is concentrated solar thermal power (CSP) which uses reflectors to focus solar radiation onto a receiver that transfers the received heat to a heat transfer fluid. One of the CSP technologies is heliostat based central power tower. The heliostats collectively focus incident sunlight onto a central receiver. On account of high concentration, temperature of the order of 1000 °C is achievable. This heat can be employed for process heat and power generation. Desert regions, like, Rajasthan receive high solar irradiation (~ 6-7 kW.hr/m^2/day) and are well suited for such a technology. However, dust poses a serious challenge in operating such a system (Gupta, 1986). High wind speed in such regions initiates saltation process (Singh et al., 2015). The lifted dust particles are carried by wind. When this wind blows over a field of heliostats, the particles get deposited on heliostats. The dust deposition reduces the reflectivity of heliostats (Niknia et al., 2012). This reduction lowers the overall heat recovery and, therefore, efficiency of the CSP plant. Therefore, if a parameter describing such a loss could be considered while designing the field itself, it would enable operating a plant under the desired condition.

With the importance of this aspect in mind, Yadav et al. (2014) investigated dust deposition on single and multiple aligned heliostat models in a wind tunnel at a Reynolds number of 60,000. The k-ε based Reynolds Averaged Navier-Stokes (RANS) approach was used for simulation. Further, flow measurement was performed around a heliostat using laser Doppler velocimetry technique. It was observed that the calculated time-averaged flow features are captured upstream and not reproduced downstream of the heliostat model with flow separation for an inclination angle of 25° with respect to horizontal surface. It was also observed that the wake region further downstream is adequately captured. Further, this investigation revealed that non-uniform or even localized dust deposition on heliostat is possible under certain condition. Localized deposition can be mitigated by cleaning effect, if predicted appropriately with a numerical tool. This investigation indicated the need for an improved modelling for analyzing air-flow around heliostats in a field layout, especially, in the flow separation region. However, it was insufficient for evaluating dust deposition on heliostats in a staggered arrangement, which is commonly employed (Falcone, 1986; Lipps and Vant-Hull, 1978; Vittitoe and Biggs, 1981). Considering these limitations, the presented paper aims at designing an experimental setup to understand the air-flow around heliostats in a field-type layout. For this purpose a step-wise strategy is adopted. The first step is a field design to simulate flow pattern around 1:10 scale-down heliostat models placed in staggered manner. For this purpose, geometric similarity of heliostat and field arrangement is adopted. In second step, different numbers of model heliostats, like, 3, 5, and 7 are organized in staggered fashion for a particular height of tower

doi:10.18086/swc.2015.04.04 Available at http://proceedings.ises.org

and latitude of location, which is Jodhpur based on the maximum elevation angle. In next step, detailed flow analysis is carried out using RANS approach to design an experimental set-up, which is capable of simulating a free-flow condition. Finally, Large Eddy Simulation (LES) is performed to understand, especially, the near-wake region behind a heliostat, which is not captured appropriately with RANS model. These steps are presented in the subsequent sections.

2. Field Design

As the starting point, a heliostat field is designed for Jodhpur (altitude ~ 26°) with 1m x 1m reflecting plate and 10m central tower height using Matlab code based on the mirror density criterion by Siala and Elayeb (2001) (see Fig. 1). This field design is intended for an indigenously developed open volumetric air receiver based 100kWth equivalent solar convective furnace system (Singh et al., 2015). In the Fig.1, heliostats are represented by circles. The diameter of the circles is equal to the diagonal of the heliostat. The designed field is extended up-to 30m in radius and span of 90°. The field consists of heliostats arranged in essential and staggered rows based on a no-blocking condition referred to by Siala and Elayeb (2001). The rows of heliostats are distributed radially into groups as shown in Fig. 1. These differ in their azimuthal and radial spacing. Rows of one group have equal azimuthal angular spacing between adjacent heliostats. It is to be noted that air-flow pattern depends on the positions, angular orientation and elevation of heliostats. The elevation and azimuthal angles are calculated (Xiudong et al., 2007) that vary with time and day. This yielded a maximum value of 65° throughout the year for 22nd of December. The designed field with the maximum elevation angle of 65° is scaled down geometrically for 1:10th size of the considered heliostats. The distances between heliostats are provided in Table 2. For flow similarity, the Reynolds number is to be maintained between actual and scaled-down heliostat models. The Re of the flow on the actual heliostat on a typical day in Jodhpur with an average of 7 m/s is ~ 421,000. To maintain Re with model-heliostat, the free stream air velocity ~ 70 m/s is required. Therefore, in future, attempts will be made to perform experiments with water at reduced velocity. The presented experimental set-up is designed for a free-stream air velocity up-to 20 m/s, which corresponds to Re ~ 132,000.

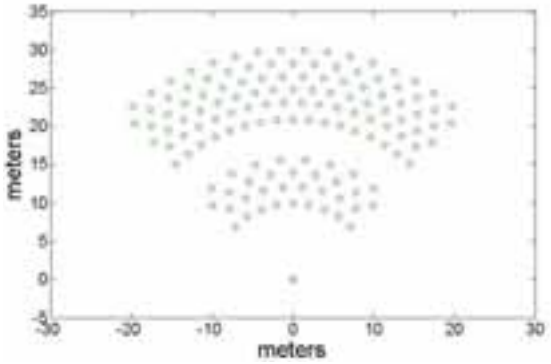

Fig. 1: Designed heliostat field

Tab. 1: Field specifications

Size of Heliostat	1 x 1 m2
Number of Heliostats	139
Tower Height	10 m
Maximum radius	30 m

Tab. 2: Scaled down distances

Between adjacent heliostats (cm)	Between rows of heliostats (cm)
20	Minimum - 17.3
	Maximum - 22.1

3. Computational Fluid Dynamics (CFD) analysis

Yadav et al. (2014) observed higher dust deposition on heliostats encountering the free stream air compared to those in the wake of preceding heliostats. The relative positioning of aligned heliostats also affected dust deposition on the aft heliostats. Following design considerations are made for experimental set-up:

a. Height and width should allow free-stream flow development from heliostat surfaces

b. The length is sufficient to allow far-wake development, indicated by a uniform velocity.

Computational Fluid Dynamics is employed to numerically solve equations of fluid flow around heliostats. The two CFD methodologies are used considering time-averaged and unsteady flow features:

3.1. Reynolds Averaged Navier-Stokes (RANS) approach

For RANS simulation, based on previous investigations, the standard two-equation k-ε model proposed by Launder and Spalding (1972) is used. This is a semi-empirical model in which turbulence kinetic energy k and

its dissipation rate ε are analyzed using their transport equations. These additional equations are solved simultaneously with governing equations of mean velocity and pressure (Kuzmin and Mierka, 2006; Furbo, 2010) for incompressible flow:

$$\nabla \bullet \overline{u} = 0 \tag{1}$$

$$\frac{\partial \overline{u}}{\partial t} + \overline{u} \bullet \nabla \overline{u} = -\nabla \overline{p} + \nabla \bullet \left(\left(\nu + \nu_T \right) \left[\nabla \overline{u} + \nabla \overline{u}^T \right] \right) \tag{2}$$

Where, ν and ν_T are molecular and turbulent eddy kinematic viscosity, respectively. The statistical eddy viscosity models the effect of unresolved velocity fluctuations in mixing. In the standard k-ε model, it is calculated by $\nu_T = C_\mu k^2 / \varepsilon$. The transport equations of k and ε in space are as follows:

$$\frac{\partial k}{\partial t} + \overline{u}_j \frac{\partial k}{\partial x_j} = \frac{\partial}{\partial x_j} \left[\left(\nu + \frac{\nu_T}{\sigma_k} \right) \frac{\partial k}{\partial x_j} \right] + \nu_T \left(\frac{\partial \overline{u}_i}{\partial x_j} + \frac{\partial \overline{u}_j}{\partial x_i} \right) \frac{\partial \overline{u}_i}{\partial x_j} - \varepsilon \tag{3}$$

$$\frac{\partial \varepsilon}{\partial t} + \overline{u}_j \frac{\partial \varepsilon}{\partial x_j} = \frac{\partial}{\partial x_j} \left(\frac{\nu_T}{\sigma_\varepsilon} \frac{\partial \varepsilon}{\partial x_j} \right) + C_{e1} \frac{\varepsilon}{k} \nu_T \left(\frac{\partial \overline{u}_i}{\partial x_j} + \frac{\partial \overline{u}_j}{\partial x_i} \right) \frac{\partial \overline{u}_i}{\partial x_j} - C_{e2} \frac{\varepsilon^2}{k} \tag{4}$$

Where, σ_k is the turbulent Prandtl number for kinetic energy. The turbulent length scale (L_0) could be obtained from k and ε as $\varepsilon = k^{3/2} / L_0$. The standard values of the model constants of the above equations are: $C_\mu = 0.09$, $C_{\varepsilon 1} = 0.09$, $C_{\varepsilon 2} = 0.09$, $\sigma_k = 1.0$, $\sigma_\varepsilon = 1.3$

3.1.1. Geometry

The employed 3-D models representing a part of the designed heliostat field using scale-down heliostat models are presented in Fig. 2a, b and c. The required minimum numbers of heliostat for staggered configuration is 3. Here, there is no heliostat with more than one adjacent heliostat in the same row (Fig. 2a). To investigate the interaction of wake from nearby heliostats, a representative field with 5 and 7 heliostats is considered (Fig. 2b, c). These layouts correspond to an elevation angle of 25°. In Fig. 2 distance between adjacent heliostats is 20 cm and the distance between two rows is 22.1 cm as in Table 2 (Yadav et al., 2014).

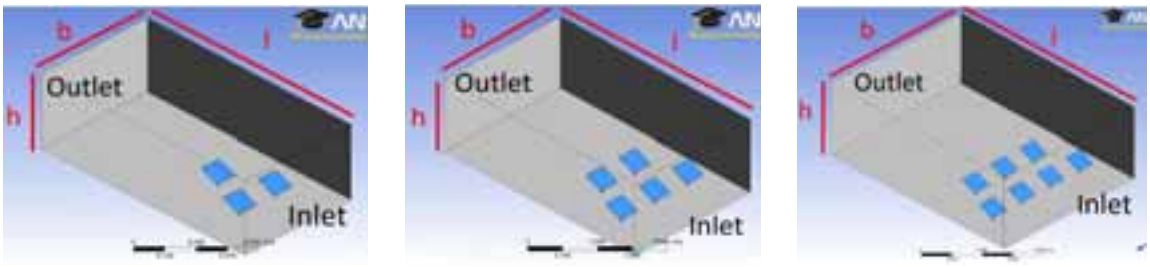

(a) **(b)** **(c)**

Fig. 2: Dimensions l x b x h =: a) 120 cm x 60 cm x 40 cm; b) 120 cm x 70 cm x 40 cm; c) 120 cm x 90 cm x 45 cm.

3.1.2. Mesh

The flow domain is discretized by dividing into smaller control volumes called mesh elements. Polyhedral mesh elements are considered. A mesh with smaller element size is said to be a finer mesh. Figure 3 shows the employed polyhedral mesh element at the middle plane of domain. CFD simulations are performed for an average mesh resolution of 1, 2, 3 & 4 mm (Table 3) on all the geometries.

Tab. 3: (a) Edge size and (b) Inflation resolution

Edge sizing (mm)
1
2
3
4

S.no	Boundary Layer	
	Over heliostat mirror	Over enclosure wall
1	0.1 mm, 1.2 growth, 7 layers	0.2 mm, 1.2 growth, 10 layers
2	0.1 mm, 1.2 growth, 7 layers	0.3 mm, 1.2 growth, 7 layers
3	0.2 mm, 1.2 growth, 4 layers	0.3 mm, 1.2 growth, 7 layers


(a)


(b)

Fig.3. a) Polyhedral mesh at the middle plane of study domain; b) Fine volume cell near heliostat geometry and inflation over wall and heliostat plate.

3.1.3. CFD set-up and Mesh dependency

The standard k-Ɛ turbulence model, elaborated earlier, using the pressure-velocity coupled SIMPLE algorithm as available in ANSYS-FLUENT 13.0 was employed for CFD analysis. The validation of adopted set-up is presented by Yadav et al. (2014) and Singh et al. (2015). Thus, no separate validation is provided in this paper. In these simulations, the considered maximum uniform axial-inlet velocity is 20 m/s with 3% turbulence intensity. For the gradient calculations, least-square scheme is employed. The first-order upwind scheme is employed for calculating momentum, kinetic energy (k) and its dissipation ($\mathcal{E}$) equations with a convergence criterion of 10^{-5}. The generated meshes for grid dependence investigation are given in Table 4.

Tab. 4: Mesh resolution

S. No.	Geometry	Mesh resolution	Avg. Y+	Mesh elements
1	3 heliostats	4 mm	3.5	1.34 million
2	5 heliostats	4 mm	5.7	2.00 million
3	7 heliostats	4 mm	5.8	3.93 million

3.2. Large Eddy Simulation (LES) approach

In large eddy simulations, the sub-grid scales are filtered out and larger scales are resolved by the adopted filter or grid resolution and analyzed. The dimensionless implicit grid-filtered Navier-Stokes equations for an incompressible fluid are given as follows:

$$\frac{\partial \overline{u}_i}{\partial x_i} = 0 \tag{5}$$

$$\frac{\partial \overline{u}_i}{\partial t} + \frac{\partial}{\partial x_j}\left(\overline{u}_i \overline{u}_j\right) = -\frac{\partial \overline{p}}{\partial x_i} - \frac{\partial \tau_{ij}}{\partial x_j} + \frac{1}{\mathrm{Re}} \frac{\partial^2 \overline{u}_i}{\partial x_j x_j} \tag{6}$$

Where, $\overline{u}_i$ is the velocity component of the resolved scales, p is the pressure and Re is the Reynolds number. The turbulence stresses, τ_{ij} represent the effects of small scales on resolved structures and proportional to the mean velocity gradients, the large-scale strain rate tensor S_{ij}:

$$\tau_{ij}^a = \tau_{ij} - \frac{\delta_{ij}}{3}\tau_{kk} = -2\mu_T \overline{S}_{ij} \tag{7}$$

Where, τ_{ij}^a is the anisotropic part of the sub-grid scale Reynolds stresses τ_{ij} and δ_{ij} is Kronecker delta. The trace of the stress tensor is usually added to the filtered pressure p. The expression for eddy viscosity μ_T determined by Smagorinsky model (Smagorinsky, 1963) is as follows:

$$\mu_T = \rho\left(C_S \Delta\right)^2 \left|\overline{S}\right| \tag{8}$$

Where, Δ is the filter width which is proportional to the grid size, ρ is the density, C_S is the Smagorinsky constant, $\left|\overline{S}\right| = \left(2\overline{S}_{ij}\overline{S}_{ij}\right)^{1/2}$ is the magnitude of large-scale strain rate tensor. Further, Germano et al. (1991) proposed a dynamics sub-grid stress model which calculates C_S as a function of space and time by using two filters, test and grid filters. In dynamics model, Lilly (1992) proposed a least squares method to calculate C_S.

3.2.1. Geometry

Due to the computationally expensive nature of LES, this simulation is conducted over a smaller geometry with only one heliostat model as shown in Fig. 4 with corresponding dimensions in Table 5. This setup is experimentally analyzed in Yadav et al. (2014). This is utilized in this paper for validation of LES approach.

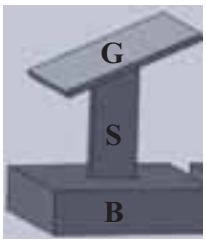

Fig. 4: Single heliostat

Tab. 5: Dimension of heliostat used in LES analysis

Component	Dimension (mm)
Glass Mirror (G)	60 x 60 x 3
Stand (S)	18 x 6 x 50
Base (B)	68 x 74 x 20

3.2.2. Mesh and CFD set-up

For the current study, sub-grid stress model is employed to simulate flow around a single heliostat with dimensions (see Table 5) as in Yadav et al. (2014). Uniform axial velocity as 16 m/s is applied at inlet with no perturbation as in the performed experiment. At walls, no slip boundary condition is used. SIMPLE algorithm is used with pressure-velocity coupling. Least-squares cell based scheme is used for gradient calculations. For continuity and momentum equations, bounded central differencing is used. The Y-plus at the heliostat plate ~ 2 (see Fig. 5b) as suggested by Davidson (2009). The total number of cells in the domain is around 1.0 Million. Fig. 5a shows the polyhedral mesh at the middle plane of the domain.

Fig. 5: (a) Polyhedral mesh at the middle plane of the domain; (b) Y-plus at the heliostat plate is ~ 2.

4. Results

4.1. RANS

Figure 6a shows various lines, namely, horizontal, longitudinal and vertical along which RANS analyzed axial-velocity is reported in Fig. 6b, c, and d. One of the representative heliostats is identified by symbol 'a'. Fig. 6b clearly depicts deceleration of axial velocity towards heliostat for the cases with 3, 5 and 7 heliostats. In these simulations the elevation angle is 25°. The arrow (→) indicates flow direction from left to right. It can be inferred that the axial-velocity, finally, develops to the maximum value, as expected, in far wake. This confirms that the considered length allows development of wake, as envisaged. The plotted time-averaged axial-velocity along the lines designated as "horizontal" and "vertical" enable tracking velocity changes. Figures 6c and 6d show that the calculated axial-velocity develops to free stream value of ~ 20 m/s near the wall along vertical and horizontal lines. Further, to evaluate whether the height of experimental set-up will allow using heliostat with the maximum elevation angle of 65°, additional calculations are performed. This is shown in Fig. 6d. This clearly indicates that the flow develops to free-stream condition over heliostat and eventually remains the same until viscous wall effect is encountered. Therefore, it can be safely stated that the considered length, breadth and height of 1700 mm x 1000 mm x 500 mm will be sufficient. However, a larger experimental domain of 2000 mm x 1200 mm x 600 mm is considered with ~ 20% safety margin. This is currently under fabrication and experimental results will be reported in near future.

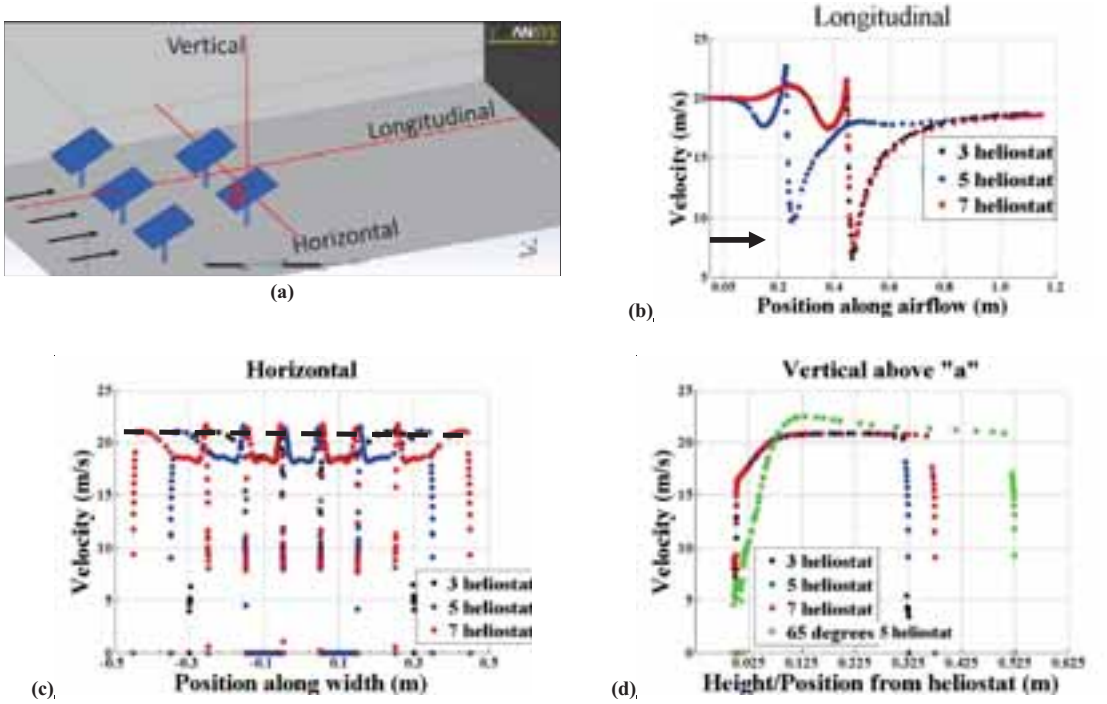

Fig. 6: (a) Geometry showing lines along which velocity is plotted. (b) Longitudinal line axial to the direction of flow, (c) Horizontal line through rear row of heliostats, (d) Vertical line above heliostat labeled "a" (including result for 65° elevation)

Velocity contours and streamlines are given in Fig. 7 for visual representation of the flow field. The velocity contour and streamlines in Fig. 7a and b clearly indicates the strongly affected region behind a heliostat. This results in formation of vortex, as expected, behind the heliostat. Figures 7c and d show the streamlines on a horizontal plane passing through the centers with 3 and 5 heliostats, respectively. Practically, no difference is observed as the wake develops eventually to free stream as depicted in Fig. 6b. However, the existence of heliostat in wake affected region may lead to its induced vibration resulting in a higher spillage loss or even distorted focus on receiver.

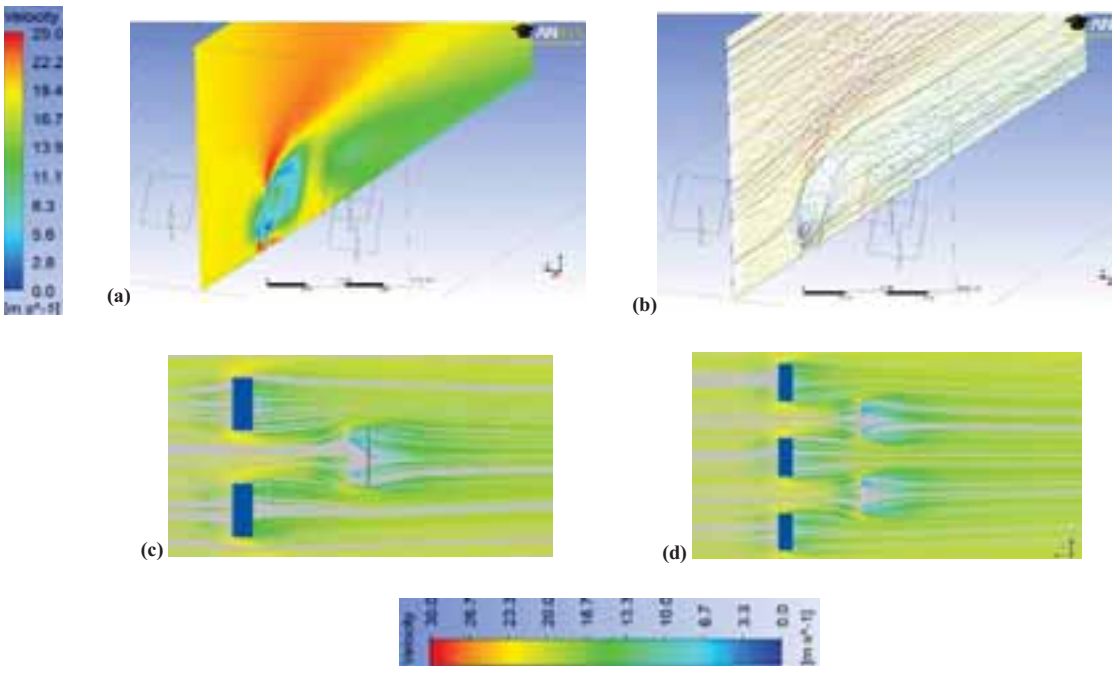

Fig. 7: (a) Velocity contour (b) Streamlines and vectors in vertical plane through a heliostat, (c) Streamlines at horizontal mid-plane through 3 heliostats and (d) through 5 heliostats

4.2. LES

It should be emphasized that RANS showed clear limitations in predicting near-wake region of heliostat. This region is characterized by high RMS values as observed in experiments. The previous studies (Breuer et al., 2003; Rodi, 1993) of flow past an inclined plate revealed that the separated flow shows complicated and highly unpredictable behavior. Obviously, the standard k-$\mathcal{E}$ model was not suitable. In order to capture the dynamic behavior of flow behind the heliostat model, LES analysis is performed using zero-equation sub-grid scale model as proposed by Germano et al. (1991). The LES analyzed instantaneous iso-surface of coherent structures for a given vorticity is shown in Fig. 8a behind the model heliostat. This is colored with velocity. These flow structures are expected to cause induced vibration and also affect the dust deposition on the subsequent heliostats. Thus, a parameter based on wake-based factor is required for field design. Fig. 8b shows the comparison between LES analyzed and measured axial-velocity using Laser Doppler Velocimetry (LDV). The velocities are plotted at seven locations, from 5 mm to 30 mm with 5 mm gap and at 200 mm from the trailing edge of the heliostat plate along the axial axis of plate, marked as 1 to 6 & 7 on horizontal axis respectively. Further, LES analyzed and experimentally estimated RMS values of axial-velocity are plotted at similar locations in Fig. 8c. It could be observed that the LES analyzed values are within ± 10% of the experimentally measured values. Thus, it can be safely stated that the performed LES provided useful details about mean and fluctuating flow quantities. However, further improvement using one-equation model is expected.

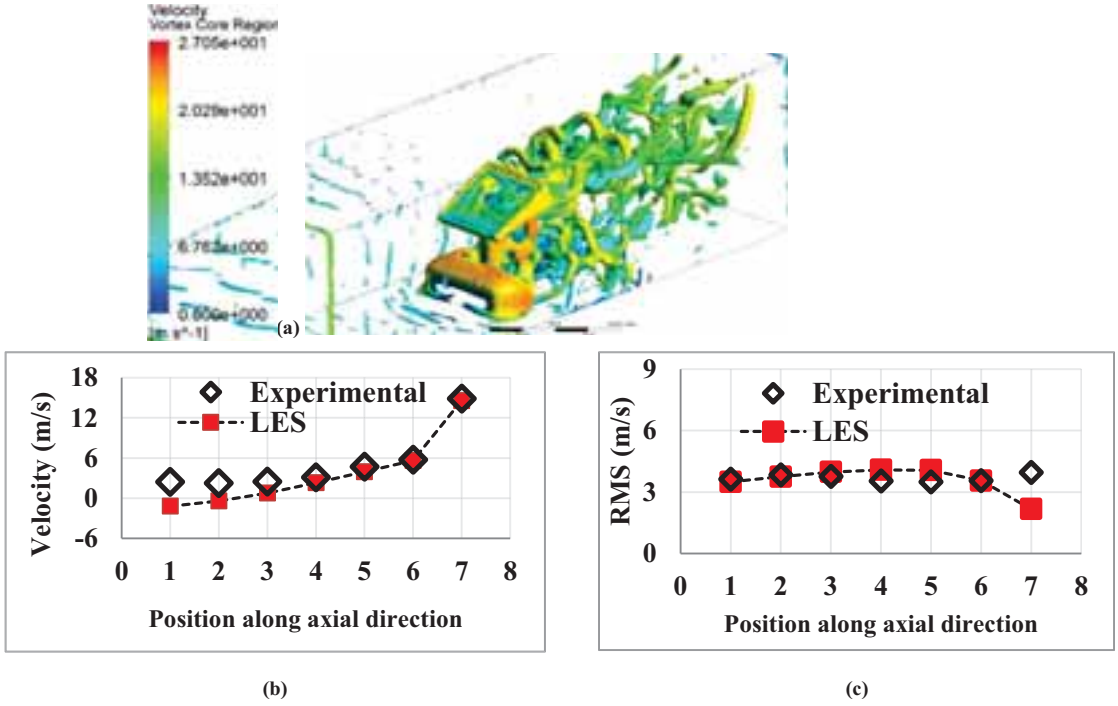

Fig. 8: (a) Coherent flow structures correspond to 620 Hz; (b) Time-averaged Mean Velocity and, (c) RMS velocity along an axial line behind the heliostat at 5, 10, 15, 20, 25, 30 & 200 mm from trailing edge represented by numbers 1 to 6 & 7, respectively.

5. Conclusion

This paper presents the design and evaluation of an experimental set-up for analysis of fluid flow and dust deposition on heliostats in a field layout. For this purpose, a basic field using scale-down heliostat models is designed using available literature. Afterwards, using the validated RANS CFD approach a detailed air-flow analysis around heliostats is performed. This reveals that even with an extreme inclination angle of 65°, an experimental domain of 2000 mm x 1200 mm x 600 mm will allow wake and flow development to free-stream values. Further, detailed LES analysis showed the presence of coherent structures behind a heliostat, which is expected to induce vibration if a heliostat is exposed. Therefore, it is concluded that correction parameters Considering the stability and safety of the operation based on wake-related and dust-deposition factors will be

required for a more realistic evaluation of field- design and performance. The designed experimental set-up is currently under fabrication and experimental results will be reported in future.

6. Acknowledgements

The authors acknowledge the received infrastructure and financial support from IIT Jodhpur and Ministry of New and Renewable Energy (MNRE) funded project vide sanction letter no. 15/40/2010-11/ST. The authors extend their thanks to Vikash Goenka for his assistance during the draft of this manuscript.

7. References

Breuer, M., Jovičić, N., Mazaev, K., 2003. Comparison of DES, RANS and LES for the separated flow around a flat plate at high inclination. Int. J. Numerical Methods Fluids 41, 357-388.

Davidson, L., 2009. Large Eddy Simulation: how to evaluate resolution. Int. J. Heat Fluid Flow 30, 1016-1025.

Falcone, P.K., 1986. A handbook for solar central receiver design. Sandia National Laboratories.

Furbo, E., 2010. Evaluation of RANS turbulence models for flow problems with significant impact of boundary layers. UPTEC F10061; Master thesis.

Germano, M., Piomelli, U., Moin, P., Cabot, W.H., 1991. A dynamic subgrid-scale eddy viscosity model, Phys. Fluids A3, 1760-1765.

Gupta J.P., 1986. Moisture and thermal regimes of the desert soils of Rajasthan, India, and their management for higher plant production. Hydrol. Sci., J. 31, 347-359.

Kuzmin, D., Mierka, O., Turek, S., 2007. On the implementation of the k−ε turbulence model in incompressible flow solvers based on a finite element discretization. Conference Int. J. of Computing Sci. and Mathematics. 1, 193-206.

Launder, B.E., Spalding, D.B., 1972. Mathematical Models of Turbulence, Academic Press, London.

Lilly, D.K., 1992. A proposed modification of the Germano subgrid-scale closure method, Phys. Fluids A4, 633-635.

Lipps, F.W., Vant-Hull, L.L., 1978. A cell-wise method for the optimization of large central receiver systems. 20, 505–516.

Niknia, I., Yaghoubi, M., and Hessami, R., 2012. A novel experimental method to find dust deposition effect on the performance of parabolic trough solar collectors. Int. J. Env. Studies, 69 (2), 233-252.

Rodi, W., 1993. On the simulation of turbulent flow past bluff bodies, J. Wind Eng. Ind. Aerodynamics 46 & 47, 3-19.

Siala, F.M.F., Elayeb, M.E., 2001. Mathematical formulation of a graphical method for a no-blocking heliostat field layout, Renewable Energy, 23(1), 77–92.

Singh, G., Saini, D., Yadav, N., Sharma, R., Chandra L., Shekhar, R., 2015. Dust deposition mechanism and cleaning strategy for open volumetric air receiver based solar tower sub-systems. Energy Procedia 69, 2081 – 2089.

Smagorinsky, J., 1963. General circulation experiments with the primitive equations, Monthly Weather Review, 91(3), 99-164.

Vittitoe, C., Biggs, F., 1981. A user's guide to helios: a computer program for modeling the optical behavior of reflecting solar concentrators, part I. Introduction and code input. Sandia National Laboratories.

Xiudong, W., Zhenwu, L., Zi, L., Hongxin, Z., Zhengguo, N., 2007. Optimization Procedure for Design of Heliostat Field Layout of a 1MWe Solar Tower Thermal Power Plant. Proc. of SPIE 6841 684119, 1–10

Yadav, N.K., Pala, D., Chandra, L., 2014. On the understanding and analyses of dust deposition on heliostat. Energy Procedia 57, 3004 – 3013.